IOP Publishing Journal of Physics: Condensed Matter
J. Phys.: Condens. Matter **32** (2020) 185601 (8pp) https://doi.org/10.1088/1361-648X/ab6be8

Thermal quantum correlations in zigzag graphene nanoribbons

Xiao-Dong Tan[1,2] **and Qian-Hui Mao**[2]

[1] School of Electronic Information and Electrical Engineering, Shangluo University, Shangluo 726000, People's Republic of China
[2] School of Science, Henan Institute of Engineering, Zhengzhou 451191, People's Republic of China

E-mail: txd10@163.com

Received 29 September 2019, revised 18 December 2019
Accepted for publication 15 January 2020
Published 4 February 2020

Abstract

Based on the effective spin-ladder model, we compute the negativity and geometric quantum discord (GQD) between two edge spins in zigzag graphene nanoribbons (ZGNRs) thermalized with a reservoir at temperature T (canonical ensemble). The results show that the entanglement only exists in antiferromagnetically coupled spin pairs, and completely vanishes between any two spins at the same ribbon edge. Intriguingly, the dominant entanglement always occurs in the nearest inter-edge coupled spin pairs, which is very robust even at room temperature. By contrast, almost all edge spin pairs can hold non-zero GQD, which strongly depends on the ribbon width. To get further insight into the properties of entanglement, the multiparticle entanglement (ME) shared between three spins is studied. The results show that ME always exists among spins located at different edges, and it is more robust than the corresponding two-spin entanglement in against the temperature. These remarkable properties make ZGNRs very promising for possible applications in quantum information processing.

Keywords: zigzag graphene nanoribbon, negativity, geometric quantum discord

(Some figures may appear in colour only in the online journal)

1. Introduction

Quantum entanglement is one of the core resources for quantum information processing, such as unconditionally secure transmission of information and high-efficiency quantum computation [1]. It has also been identified and extensively studied in human cognitive processes nowadays [2]. However, entanglement is not the only form of nonclassical correlation in a given system. It has become clear that some separable mixed states also hold nonclassical correlations, which are responsible for the speedup in deterministic quantum computation with one pure qubit (DQC1) [3, 4]. Thus, the research of such quantum correlations in a given state is one of the imperative tasks related to understanding the quantum nature of a state and efficient utilization of the state for quantum information processing. A great deal of works have been done to investigate the potential applications of these quantum correlations, including remote state preparation [5–7], state discrimination [8, 9], dense coding [10–13], quantum computation [14, 15], and quantum internet [16–18]. To successfully achieve these applications in reality, finding ideal quantum materials is an essential prerequisite.

Graphene [19], a 2D honeycomb lattice of carbon, is regarded as a promising candidate owing to its weak intrinsic spin-orbit coupling and completely vanishing hyperfine interaction [20]. Thus, it has attracted a rise of interest on various quantum properties of graphene, such as spin qubits [21, 22], quantum dynamics [23], quantum interference [24, 25], quantum ripples [26], quantum refrigerators [27], and nonlinear quantum optical properties [28]. Remarkably, several schemes to achieve quantum computing in graphene-based systems have been studied and reported [29–32]. One of the interesting nanostructures of graphene is called the zigzag graphene nanoribbon (ZGNR). It possesses spin-polarized edge states, which serve as key elements for graphene-based spintronics devices [33, 34]. The edge spins in ZGNRs were predicted to couple ferromagnetically along the each edge and antiferromagnetically between the opposite edges. And the atomically precise ZGNRs have been synthesized through surface-assisted polymerization and cyclodehydrogenation of

specifically designed precursor monomers [35]. Several works have been done to explore quantum effect in ZGNRs, for examples, quantum transport [36], quantum spin Hall effect [37], and adiabatic quantum pump effect [38, 39]. Based on the effective low-energy theory [40], Koop *et al* derived an effective spin-ladder model for ZGNRs [41], and further investigated the quantum phase transitions in ZGNRs [42]. Intriguingly, Hagymási *et al* showed that for ZGNRs besides the strong nearest-neighbor entanglement, moderately strong entanglement appears between the two edges, and between electrons on the same edge [43]. However, electron spins on the same edge are ferromagnetically coupled, and whether entanglement exists in such edge states or not needs more evidence to confirm. Moreover, from the practical standpoint, understanding the quantum correlation structure in ZGNRs is important for their future applications in quantum information processing.

In this paper, we employ the effective spin-ladder model to investigate the negativity and geometric quantum discord (GQD) in ZGNRs. First, we study the behaviors of quantum correlations in all edge spin pairs at $T = 0$. Results show that negativity only exists in the inter-edge coupled spin pairs, and the dominant entanglement always occurs in the pair of nearest abreast spins across the ribbon. Compared with negativity, almost all edge spin pairs could have non-zero GQD. Both negativity and GQD strongly depend on the ribbon width and relative location between two considered spins. In particular, the robustness of entanglement and GQD against temperature will be shown. Finally, we focus on multiparticle entanglement (ME) shared in such many-body system, where the entanglement between one spin and the other two will be discussed emphatically.

2. Definitions of measuring quantum correlations

For spin-1/2 systems, an arbitrary bipartite state ρ_{AB} can be expressed in Bloch representation,

$$\rho_{AB} = \frac{1}{4}\left(I\otimes I + \sum_{i=1}^{3} x_i\sigma_i\otimes I + \sum_{i=1}^{3} y_i I\otimes\sigma_i + \sum_{i,j=1}^{3} T_{ij}\sigma_i\otimes\sigma_j\right), \tag{1}$$

where $x_i = \mathrm{tr}(\rho_{AB}\sigma_i\otimes I)$, $y_i = \mathrm{tr}(\rho_{AB}\sigma_i\otimes I)$, $T_{ij} = \mathrm{tr}(\rho_{AB}\sigma_i\otimes\sigma_j)$, and σ_i, $i\in\{x,y,z\}$ are three Pauli matrices. To quantify the total quantum correlation in the bipartite state ρ_{AB}, Dakić *et al* introduced the GQD, which is defined as [44]

$$D_{\mathrm{G}}(\rho_{AB}) \equiv \underset{\chi_{AB}\in\Omega_0}{\mathrm{Min}} \|\rho_{AB}-\chi_{AB}\|^2, \tag{2}$$

where Ω_0 denotes the set of all zero-discord states, the minimization is taken over all states χ_{AB} belonging to Ω_0, and $\|X-Y\|^2 = \mathrm{tr}(X-Y)^2$ is the square norm in the Hilbert-Schmidt space. Compared with quantum discord (QD) introduced by Ollivier *et al*, GQD is easy to compute and its explicit expression for the case of two qubits is given by

$$D_{\mathrm{G}}(\rho_{AB}) = \frac{1}{4}(\|\vec{x}\|^2 + \|T\|^2 - k_{\max}), \tag{3}$$

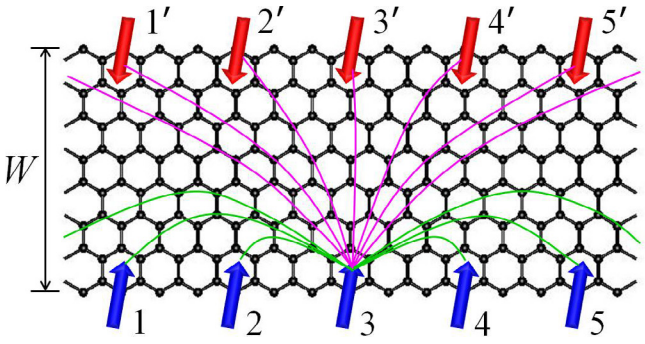

Figure 1. Lattice geometry of a zigzag graphene nanoribbon with $W = 8$ zigzag lines across the ribbon. Such system can be mapped into an effective spin-ladder model, where the effective spin–spin interactions are ferromagnetic (antiferromagnetic) along (across) the edges and sketched here for one reference spin '3'.

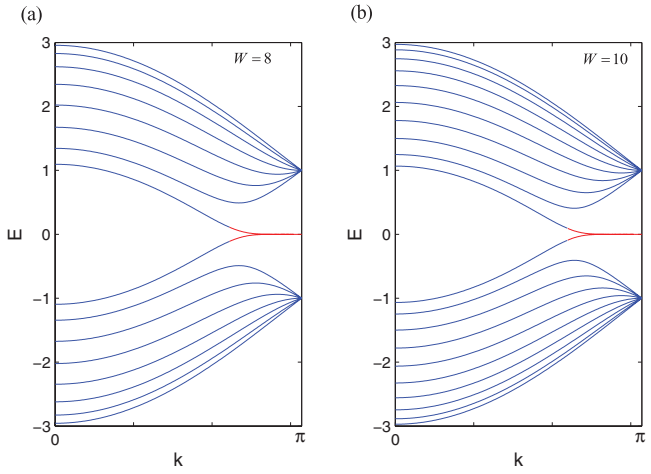

Figure 2. The tight-binding-model band structures for ZGNRs with (a) $W = 8$ and (b) $W = 10$, respectively. The red part of the flat bands belongs to the edge states within the region $2\pi/3 \leqslant |k| \leqslant \pi$.

where $k_{\max}$is the largest eigenvalue of matrix $K = \vec{x}\vec{x}^T + TT^T$.

In order to analyze the entanglement, we use the negativity as the measurement, which is defined as [45]

$$N(\rho_{AB}) \equiv \frac{\left\|\rho_{AB}^{T_A}\right\|_1 - 1}{2} = \sum_i |\mu_i|, \tag{4}$$

where $\rho_{AB}^{T_A}$ is the partial transpose of the density matrix ρ_{AB} with respect to subsystem A, $\left\|\rho_{AB}^{T_A}\right\|_1 = \mathrm{tr}\sqrt{(\rho_{AB}^{T_A})^{\dagger}\rho_{AB}^{T_A}}$ is the trace norm of $\rho_{AB}^{T_A}$, and μ_i are the negative eigenvalues of $\rho_{AB}^{T_A}$. Note that negativity is a good detector for two-particle entanglement and ME, but it is invalid for positive partial transpose entangled states.

3. Two-spin entanglement and GQD in ZGNRs

The geometry of ZGNR is shown in figure 1. For ZGNRs, the electronic states with nearly zero energy are localized at the ribbon edge (so-called edge states), and give rise to a flat band extending over one-third of the 1D Brillouin zone within the region $2\pi/3 \leqslant |k| \leqslant \pi$, as shown in figure 2. The flatness of

Table 1. Values of spin coupling coefficients in the effective spin-ladder model for ZGNRs with $U = t$ and $W = 6$, 8, 10, and 12, respectively. The data are from [48].

r $(W = 6)$	$J_{\rm F}(r)/t$	$J_{\rm AF}(r)/t$
0		0.09 702 854
1	–0.04 589 570	0.06 249 864
2	–0.00 545 912	0.01 750 839
r $(W = 10)$	$J_{\rm F}(r)/t$	$J_{\rm AF}(r)/t$
0		0.01 964 170
1	–0.04 539 141	0.01 558 524
2	–0.00 474 753	0.00 798 144
r $(W = 8)$	$J_{\rm F}(r)/t$	$J_{\rm AF}(r)/t$
0		0.04 034 668
1	–0.04 549 982	0.02 958 178
2	–0.00 494 775	0.01 207 769
r $(W = 12)$	$J_{\rm F}(r)/t$	$J_{\rm AF}(r)/t$
0		0.01 238 082
1	–0.04 537 878	0.01 034 815
2	–0.00 466 976	0.00 614 887

the energy distribution of the edge states leads to a high local density of states at the Fermi energy. Since the edge states are responsible for the edge magnetism, thus the edge states play an important role in the magnetic properties of ZGNRs. The on-site Coulomb repulsion between electrons splits degenerate edge states into spin-polarized bands, opening a band gap across the whole flat-band segment [46, 47]. According to [41], such magnetic interactions at the edges of ZGNRs can be described by the effective spin-ladder model,

$$H_{eff} = -\sum_{i<j,s} J_{ij}^{F}\vec{\sigma}_{is}\cdot\vec{\sigma}_{js} + \sum_{ij} J_{ij}^{AF}\vec{\sigma}_{iU}\cdot\vec{\sigma}_{jL}, \tag{5}$$

where periodic boundary conditions are assumed, $\vec{\sigma}_{js}$ denotes the vector of Pauli operator on the jth rung of the ladder at one leg $s = U$ (L), $J_{ij}^{F}$is the ferromagnetic coupling for spins located at the same edge, and $J_{ij}^{AF}$is the antiferromagnetic coupling between spins at the different edges. Due to the translational symmetry, these couplings depend on the relative distance $(r = |i-j|)$ between spins, i.e. $J_{ij}^{F} = J_{F}(r)/4$ and $J_{ij}^{AF} = J_{AF}(r)/4$. The method to calculate these coupling coefficients $J_{(A)F}(r)$ is complicated and onerous (for more details see [41, 48]). As for leading order terms, the ferromagnetic couplings scale proportional to the on-site Coulomb repulsion U, and the antiferromagnetic couplings scale with t^2/U, where $t \approx 3\,\mathrm{eV}$ is the nearest-neighbor hopping amplitude. Following the [42], we choose $U = t$ throughout this paper. Here four different width ZGNRs ($W = 6$, 8, 10, and 12) are considered, where the effective couplings are given in table 1.

The density operator for the system (5) in equilibrium with a thermal reservoir is given by

$$\rho = \frac{1}{Z}\exp(-\beta H_{\rm eff}), \tag{6}$$

where $\beta = 1/k_{\rm B}T$, $k_{\rm B}$ is Boltzmann's constant, T is the absolute temperature, and $Z = \mathrm{tr}\,\exp(-\beta H_{\rm eff})$ is the partition function. Then, the reduced density operator for two spins at sites i and j, is obtained by tracing all but two considered spins,

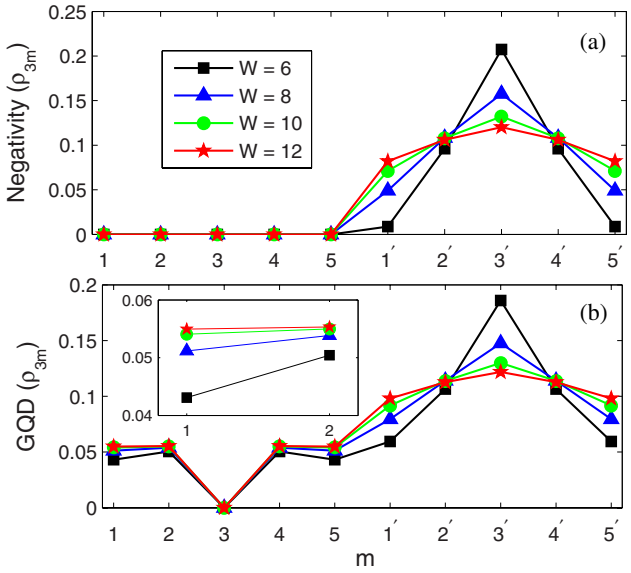

Figure 3. (a) Negativity and (b) GQD as a function of the edge site m in ZGNRs with $U = t$, for $W = 6$, 8, 10, and 12, respectively. The inset shows GQD for states ρ_{31} andρ_{32}.

$$\rho_{ij} = \mathrm{tr}_{N-2}(\rho). \tag{7}$$

Due to the translation invariance and $U(1)$ invariance ($[H,\ \sum_{n=1}^{N}\sigma_n^z] = 0$) of the Hamiltonian (5), the density matrix for state ρ_{ij} must have the form

$$\rho_{ij} = \frac{1}{4}\left(I\otimes I + g_1\sigma_i^x\otimes\sigma_j^x + g_2\sigma_i^y\otimes\sigma_j^y + g_3\sigma_i^z\otimes\sigma_j^z\right), \tag{8}$$

with $g_1 = \mathrm{tr}\left(\sigma_i^x\sigma_j^x\rho\right)$, $g_2 = \mathrm{tr}\left(\sigma_i^y\sigma_j^y\rho\right)$, and $g_3 = \mathrm{tr}\left(\sigma_i^z\sigma_j^z\rho\right)$. Note that

$$g_1 = g_2 = g_3 = g(i,j), \tag{9}$$

owing to the isotropy of exchange interactions, and $g(i,j) = g(|i-j|) = g(r)$ because of the translational symmetry along the ribbon. After straightforward calculations, we obtain

$$D_{\rm G}(\rho_{ij}) = \frac{g(r)^2}{2}, \tag{10}$$

$$N(\rho_{ij}) = \begin{cases} -\,[1+3g(r)]/4, & (-1 < g(r) < -1/3) \\ 0, & (-1/3 \leqslant g(r) < 1) \end{cases}, \tag{11}$$

which depend on the relative location between two considered spins. Thus, we only need to fix one edge site as the reference point in the following discussions, and quantum correlations relative to the other reference sites are self-evident. For convenience, here we choose the site '3' as the reference point.

We first focus on the pairwise entanglement and GQD in different width ZGNRs at zero temperature, as shown in figure 3. We can see that there is no entanglement between any two spins at the same edge, and entanglement always occurs in inter-edge coupled spin pairs (see figure 3(a)), where the dominant entanglement always occurs in the pair of nearest abreast spins across the ribbon. Interestingly, negativity for state $\rho_{33'}$ always decreases with the increasing ribbon width, while for

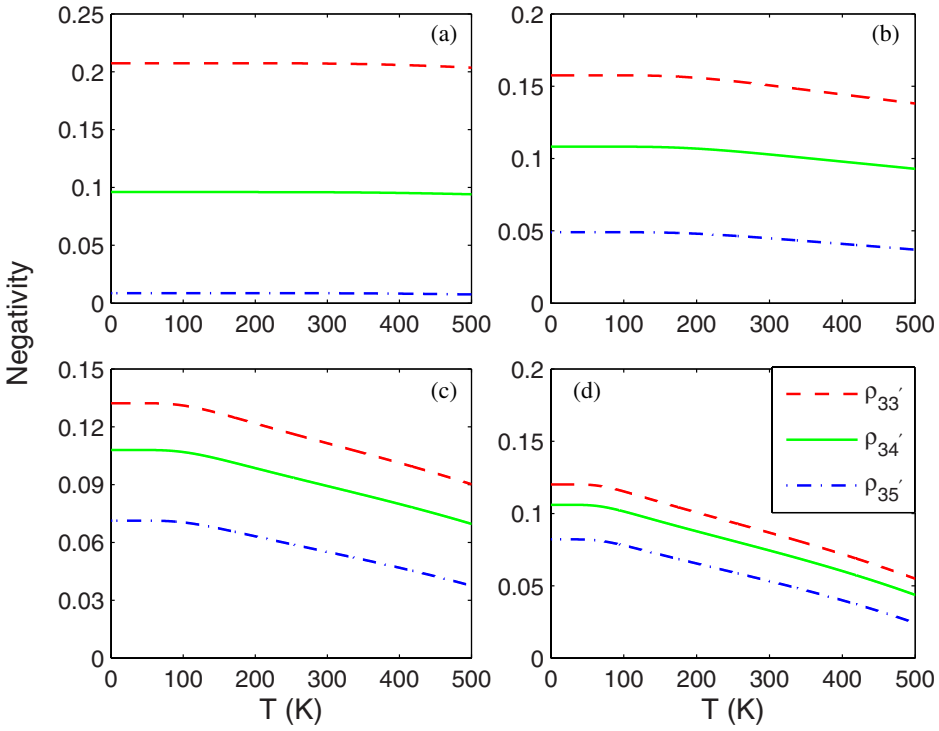

Figure 4. Negativity for different states $\rho_{33'}$, $\rho_{34'}$, and$\rho_{35'}$, as a function of temperature T in ZGNRs with (a) $W = 6$, (b) $W = 8$, (c) $W = 10$, and (d) $W = 12$, respectively.

state $\rho_{31'}$ or $\rho_{3,5'}$ negativity just displays the opposite behavior. Compared with negativity, all the edge spin pairs considered here hold non-zero GQD (see figure 3(b)). And GQD for intra-edge coupled spin pairs increases with the increasing ribbon width, due to the reduction of antiferromagnetic suppression on the long range ferromagnetic order of system.

Figure 4 shows the thermal entanglement for different width ZGNRs. We can see that the thermal entanglement (TE) for the narrow ribbons is robust in against the temperature influence, and nearly keeps a constant even at room temperature, as shown in figures 4(a) and (b). For wide ribbons, TE visibly decreases with the increasing temperature (see figures 4(c) and (d)). These results could be understood by comparing the spin coupling strength with thermal fluctuations. When the temperature is low, the thermal fluctuations are trivial and the spin exchange couplings dominate system's physical properties. While the temperature rises to a high value, behaviors of the system are then governed by thermal fluctuations. To determine the dominant magnetic order of system, the total spin coupling energy $E^{\mathrm{W}}_{\mathrm{tot}} = E_{\mathrm{FM}} + E_{\mathrm{AF}}$ is calculated according to the Hamiltonian (5) and table 1. The results show that $E^{6}_{\mathrm{tot}} = 0.5787\,\mathrm{eV}$, $E^{8}_{\mathrm{tot}} = 0.0854\,\mathrm{eV}$, $E^{10}_{\mathrm{tot}} = -0.1256\,\mathrm{eV}$, and $E^{12}_{\mathrm{tot}} = -0.2052\,\mathrm{eV}$ for $W = 6$, 8, 10, and 12, respectively. $E^{6}_{\mathrm{tot}} > E^{8}_{\mathrm{tot}} > 0$ indicates that the system mainly displays the antiferromagnetic order, which is responsible for the robustness of TE in the narrow ribbons. For $W = 10$ and 12 ZGNRs, the ferromagnetic order plays a central role, and TE becomes sensitive to the increasing temperature. For example, when $W = 12$ the antiferromagnetic coupling between two nearest-neighbor spins is $J^{\mathrm{AF}} \approx 0.1t/4 \approx 100\,\mathrm{K} \cdot k_{\mathrm{B}}$, which suggests that if $T > 100\,\mathrm{K}$ the thermal fluctuations will significantly influence TE.

Similar to TE, GQD for antiferromagnetically coupled spin pairs also declines with the increasing temperature, and the decay rate is related to the ribbon width. In this circumstance, GQD for $W = 6$ and 8 ZGNRs shows a wide plateau at room temperature (see figures 5(a) and (b)), due to the protection of the strong antiferromagnetic inter-edge couplings against the thermal noise effect. When the ribbon width increases, the thermal fluctuations rise to center stage, and thus the plateau tends to shrink for the high temperature, as shown in figures 5(c) and (d). Interestingly, GQD for ferromagnetically coupled spin pairs always shows a wide plateau even at higher temperature. So, we predict that the pairwise GQD for separable states in ZGNRs is more robust in against the thermal fluctuations than that for entangled states.

4. ME in ZGNRs

To get further insight into the distribution of entanglement in ZGNRs, we discuss the properties of ME. Here we focus on the type of bipartite entanglement between one edge spin and the other two located at the opposite edge, with respect to all possible bipartitions. The reduced density operator for three spins can be expressed in terms of three-point correlation functions, i.e.

$$\rho_{ijk} = \frac{1}{8}\sum_{\mu,\nu,\lambda}\left\langle \sigma_i^{\mu}\sigma_j^{\nu}\sigma_k^{\lambda}\right\rangle\left(\sigma_i^{\mu}\otimes\sigma_j^{\nu}\otimes\sigma_k^{\lambda}\right), \tag{12}$$

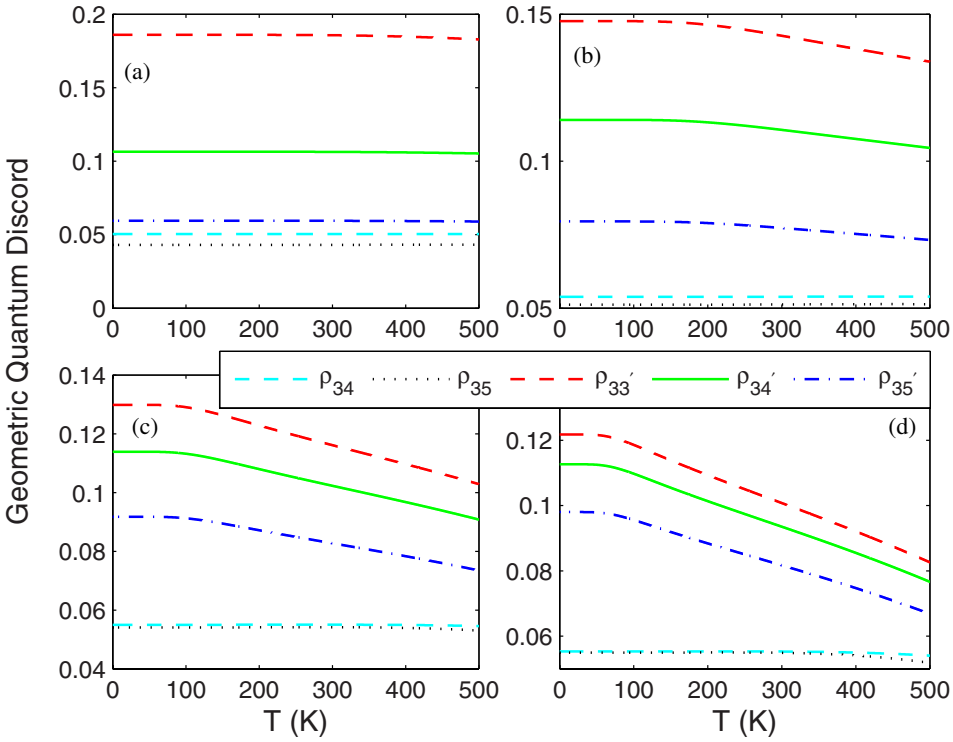

Figure 5. GQD for different states ρ_{34}, ρ_{35}, $\rho_{33'}$, $\rho_{34'}$, and$\rho_{35'}$, as a function of temperature T in ZGNRs with (a) $W = 6$, (b) $W = 8$, (c) $W = 10$, and (d) $W = 12$, respectively.

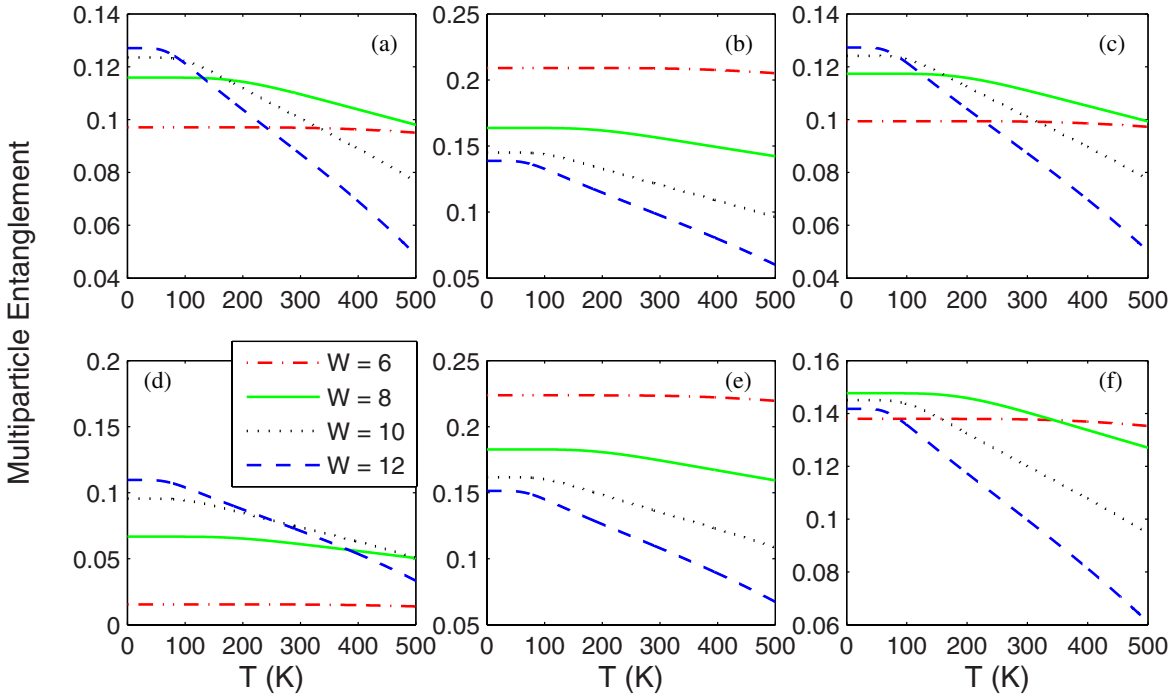

Figure 6. ME for different states (a) $\rho_{3|4'5'}$, (b) $\rho_{3|3'5'}$, (c) $\rho_{3|2'5'}$, (d) $\rho_{3|1'5'}$, (e) $\rho_{3|3'4'}$, and (f) $\rho_{3|2'4'}$, as a function of temperature T in ZGNRs with $W = 6$, 8, 10, and 12, respectively.

where $\langle \sigma_i^\mu \sigma_j^\nu \sigma_k^\lambda \rangle = \mathrm{tr}\left(\sigma_i^\mu \sigma_j^\nu \sigma_k^\lambda \rho\right)$, and μ, ν, $\lambda = 0$, x, y, z ($\sigma^0 = I$). By numerical calculation, the bipartite entanglement between one spin and the two at the opposite edge is obtained in terms of equation (4), as shown in figure 6. We can see that ME shared between three spins decays fast when temperature surpasses a certain value, and the decay rate increases with the increasing ribbon width. Compared with two-spin entanglement in figure 4, ME shared between the corresponding three spins is more robust. By meticulously comparing figures 6(a)–(f), we find that at low temperature ME persists a

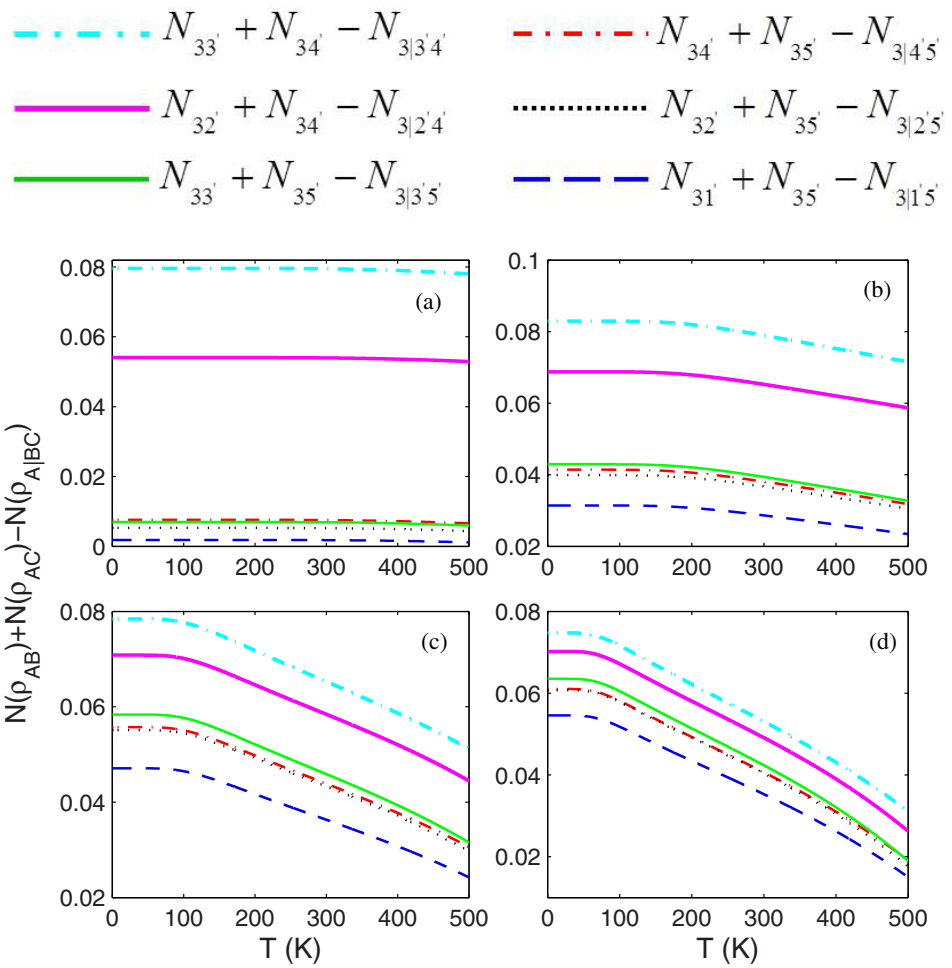

Figure 7. The gap between ME and the corresponding two-spin entanglement as a function of temperature T in ZGNRs with (a) $W = 6$, (b) $W = 8$, (c) $W = 10$, and (d) $W = 12$, respectively.

plateau, which is shrunken as the ribbon becomes wider. For states $\rho_{3|4'5'}$, $\rho_{3|2'5'}$, and $\rho_{3|1'5'}$, the plateau steps up with the increasing ribbon width when $T < 80\,\mathrm{K}$, as shown in figures 6(a), (c) and (d). While for states $\rho_{3|3'5'}$ and $\rho_{3|3'4'}$, ME just displays the opposite behaviors (see figures 6(b) and (e)). Interestingly, for the narrow ribbon, ME exhibits a wide plateau even above room temperature, whereas the plateau of ME for state $\rho_{3|2'4'}$ with $W = 8$ rises to the top at low temperature (see figure 6(f)), which is different from the other states. As can be seen in figures 6(a) and (c), ME for states $\rho_{3|4'5'}$ and $\rho_{3|2'5'}$ almost presents the same behavior, but the meticulous comparison shows that the relation $N(\rho_{3|2'5'}) \geqslant N(\rho_{3|4'5'})$ is always true for the ZGNR samples considered here, and figure 7 further confirms this result.

In figure 7, we numerically compared the difference between ME and the corresponding two-spin entanglement. According to the discussions in section 3, the spin A at one edge is separately entangled with spins B and C at the opposite edge, with the nonzero negativities N_{AB} and N_{AC}, but there exist no entanglement between B and C ($N_{\mathrm{BC}} = 0$) in ZGNR samples. By careful comparison, we found that ME shared between A and block B–C ($N_{\mathrm{A|BC}}$) is always bigger than N_{AB} and N_{AC}. While combining N_{AB} with N_{AC}, the sum ($N_{\mathrm{AB}} + N_{\mathrm{AC}}$) is always larger than $N_{\mathrm{A|BC}}$. As can be seen in figure 7(a), the gap $\Delta(\rho_{\mathrm{A|BC}}) = N_{\mathrm{AB}} + N_{\mathrm{AC}} - N_{\mathrm{A|BC}}$ for the narrow ZGNR is nearly a constant even above room temperature. For wide ZGNRs, $\Delta(\rho_{\mathrm{A|BC}})$ decays visibly with the increasing temperature, and its decay rate tends to increase with the increasing ribbon width (see figures 7(b)–(d)). Moreover, for these ZGNR samples the gap approximately satisfies the following descending order: $\Delta(\rho_{3|3'4'}) > \Delta(\rho_{3|2'4'}) > \Delta(\rho_{3|3'5'}) > \Delta(\rho_{3|4'5'}) > \Delta(\rho_{3|2'5'}) > \Delta(\rho_{3|1'5'})$.

5. Conclusion and outlook

In summary, we explored the properties of the pairwise quantum correlations in ZGNRs, i.e. negativity and GQD. The results show that there is no entanglement between any two spins at the same edge, but it is allowed to exist in antiferromagnetically coupled spin pairs. Moreover, the entanglement for nearest inter-edge coupled spin pairs is always bigger than any other cases. Compared with entanglement, almost all edge spin pairs can hold non-zero GQD. And GQD for intra-edge coupled spin pairs increases with the increasing ribbon width. Considering the thermal effect, entanglement and GQD always declines with the increasing temperature. Interestingly, GQD for ferromagnetically coupled spin pairs shows a wide

plateau even at high temperature, which are related to competition between the spin coupling interactions and thermal fluctuations. Further, we meticulously compared the two-spin entanglement with the corresponding ME. The results show that ME ($N_{\mathrm{A|BC}}$) between the spin A at one edge and spin block B–C at the opposite edge is bigger than the corresponding two-spin entanglement N_{AB} and N_{AC} ($N_{\mathrm{BC}} = 0$), but $N_{\mathrm{A|BC}} < N_{\mathrm{AB}} + N_{\mathrm{AC}}$ in ZGNRs. In addition, ME is more robust than two-spin entanglement in against the temperature.

All the results here are concluded from the pristine ZGNRs. However, the real samples of ZGNRs always contain vacancy defects or impurities. It was shown that vacancy defects [49–54] or impurities [55–58] can induce local magnetic moments in graphene and graphene ribbons. Such local magnetic moments have significant influences on the physical properties of graphene. Based on the first principles calculations, Huang *et al* demonstrated that the spin polarization will be suppressed with the increasing concentration of vacancy defects or impurities at the edges of ZGNRs [59]. So, we can predict that quantum correlations probably decrease to zero when the concentration of edge vacancy defects or impurities exceeds a critical value. It was also found that the edge states in ZGNRs are susceptible to strain [60], bending [61], corrugation [62], electric field [63], and the location of the vacancies [54] or substitutional dopants [56–58] relative to the ribbon edges. As the charge carrier density can be controlled experimentally by gate voltage, thus Fermi level in ZGNR could be shifted under the electric field, which will lead to spin suppression due to the reduction and removal of edge states at the Fermi energy. Therefore, these factors must have important influences on the quantum correlations in ZGNRs. We will systemically investigate these issues in future work.

Acknowledgments

We are grateful to Cornelie Koop for useful discussions. This work was supported by the National Natural Science Foundation of China (Nos. 11847042 and 11947003).

ORCID iDs

Xiao-Dong Tan https://orcid.org/0000-0001-5856-5635
Qian-Hui Mao https://orcid.org/0000-0002-2366-207X

References

[1] Nielsen M A and Chuang I L 2002 *Quantum Computation and Quantum Information* (Cambridge: Cambridge University Press)
[2] Aerts D, Arguëlles J A, Beltran L, Geriente S, De Bianchi M S, Sozzo S and Veloz T 2019 *Eur. Phys. J. Plus* **134** 493
[3] Knill E and Laflamme R 1998 *Phys. Rev. Lett.* **81** 5672
[4] Ali M 2014 *Int. J. Quantum Inf.* **12** 1450037
[5] Xiang G Y, Li J, Yu B and Guo G C 2005 *Phys. Rev.* A **72** 012315
[6] Dakić B *et al* 2012 *Nat. Phys.* **8** 666
[7] Ra Y, Lim H and Kim Y 2016 *Phys. Rev.* A **94** 042329
[8] Chefles A 2000 *Contemp. Phys.* **41** 401
[9] Clarke R B M, Chefles A, Barnett S M and Riis E 2012 *Phys. Rev.* A **63** 040305
[10] Mattle K, Weinfurter H, Kwiat P G and Zeilinger A 1996 *Phys. Rev. Lett.* **76** 4656
[11] Aram H, Patrick H and Debbie L 2004 *Phys. Rev. Lett.* **92** 187901
[12] Ye Y and Wee Kang C 2006 *Phys. Rev. Lett.* **96** 060502
[13] Das T, Prabhu R, De A S and Sen U 2014 *Phys. Rev.* A **90** 022319
[14] Ding S C and Jin Z 2007 *Chin. Sci. Bull.* **52** 2161
[15] Lanyon B P, Barbieri M, Almeida M P and White A G 2008 *Phys. Rev. Lett.* **101** 200501
[16] Kimble H J 2008 *Nature* **453** 1023
[17] Caleffi M, Cacciapuoti A S and Bianchi G 2018 *Proc. 5th ACM Int. Conf. on Nanoscale Computing and Communication, NANOCOM '18* (https://doi.org/10.1145/3233188.3233224)
[18] Gyongyosi L and Imre S 2018 *Sci. Rep.* **8** 10620
[19] Geim A K and Novoselov K S 2007 *Nat. Mater.* **6** 183
[20] Trauzettel B, Bulaev D, Loss D and Burkard G 2007 *Nat. Phys.* **3** 192–6
[21] Recher P and Trauzettel B 2010 *Nanotechnology* **21** 302001
[22] Chen C C and Chang Y C 2015 *Phys. Rev.* B **92** 245406
[23] Cervetti C, Rettori A, Pini M G, Cornia A, Repollés A, Luis F, Dressel M, Rauschenbach S, Kern K and Burghard M 2016 *Nat. Mater.* **15** 164
[24] Fillion-Gourdeau F, Gagnon D, Lefebvre C and MacLean S 2016 *Phys. Rev.* B **94** 125423
[25] Gehring P, Sadeghi H, Sangtarash S, Lau C S, Liu J, Ardavan A, Warner J H, Lambert C J, Briggs G A D and Mol J A 2016 *Nano Lett.* **16** 4210
[26] Hasik J, Tosatti E and Martonak R 2018 *Phys. Rev.* B **97** 140301
[27] Mani A and Benjamin C 2018 *J. Phys. Chem.* C **123** 22858–64
[28] Semnani B, Majedi A H and Safavi-Naeini S 2016 *J. Opt.* **18** 035402
[29] Wu G Y, Lue N Y and Chang L 2011 *Phys. Rev.* B **84** 195463
[30] Dragoman D and Dragoman M 2015 *Nanotechnology* **26** 485201
[31] Foulger I, Gnutzmann S and Tanner G 2015 *Phys. Rev.* A **91** 062323
[32] Chiu L K 2018 arXiv:1804.02870
[33] Kheirabadi N, Shafiekhani A and Fathipour M 2014 *Superlattices Microstruct.* **74** 123
[34] Han W, Kawakami R K, Gmitra M and Fabian J 2014 *Nat. Nanotechnol.* **9** 794
[35] Ruffieux P *et al* 2016 *Nature* **531** 489
[36] Pi S T, Dou K P, Tang C S and Kaun C C 2015 *Carbon* **94** 196
[37] Jun-Won R and Moon K 2013 *Int. J. Mod. Phys.* B **27** 1362011
[38] Zhang L 2015 *Chin. Phys.* B **24** 117202
[39] Grichuk E S and Manykin E A 2011 *JETP Lett.* **93** 372
[40] Schmidt M J, Golor M, Lang T C and Wessel S 2013 *Phys. Rev.* B **87** 245431
[41] Koop C and Schmidt M J 2015 *Phys. Rev.* B **92** 125416
[42] Koop C and Wessel S 2017 *Phys. Rev.* B **96** 165114
[43] Hagymasi I and Legeza Ö 2016 *Phys. Rev.* B **94** 165147
[44] Borivoje D, Vlatko V and Caslav B 2010 *Phys. Rev. Lett.* **105** 190502
[45] Vidal G and Werner R F 2002 *Phys. Rev.* A **65** 032314
[46] Yazyev O V 2010 *Rep. Prog. Phys.* **73** 056501
[47] Wakabayashi K, Sasaki K, Nakanishi T and Enoki T 2010 *Sci. Technol. Adv. Mater.* **11** 054504
[48] Koop C 2018 Effective Quantum Spin Models for Graphene Nanoribbons *MSc Thesis* RWTH Aachen University
[49] Vozmediano M A H, López-Sancho M P, Stauber T and Guinea F 2005 *Phys. Rev.* B **72** 155121
[50] Yazyev O V and Helm L 2007 *Phys. Rev.* B **75** 125408
[51] Palacios J J, Fernández-Rossier J and Brey L 2008 *Phys. Rev.* B **77** 195428

[52] Nair R R, Sepioni M, Tsai I, Lehtinen O, Keinonen J, Krasheninnikov A V, Thomson T, Geim A K and Grigorieva I V 2012 *Nat. Phys.* **8** 199
[53] Chen J J, Wu H, Yu D and Liao Z 2014 *Nanoscale* **6** 8814
[54] Tarawneh K and Al-Aqtash N 2014 *J. Nano Res.* **27** 65
[55] Krasheninnikov A V, Lehtinen P O, Foster A S, Pyykkö P and Nieminen R M 2009 *Phys. Rev. Lett.* **102** 126807
[56] Yu G, Lv X, Zheng Y and Tian W 2012 *J. Appl. Phys.* **111** 033707
[57] Hu X, Zhang W, Sun L and Krasheninnikov A V 2012 *Phys. Rev.* B **86** 195418
[58] Hu X, Wan N, Sun L and Krasheninnikov A V 2014 *J. Phys. Chem.* C **118** 16133
[59] Huang B, Liu F, Wu J, Gu B L and Duan W 2008 *Phys. Rev.* B **77** 153411
[60] Yang G, Li B, Zhang W, Ye M and Ma T 2017 *J. Phys.: Condens. Matter* **29** 365601
[61] Hu X, Sun L and Krasheninnikov A V 2012 *Appl. Phys. Lett.* **100** 263115
[62] Tan X D, Liao X and Sun L 2017 *Physica* E **85** 302
[63] Nomura T, Yamamoto D and Kurihara S 2010 *J. Phys.: Conf. Ser.* **200** 062015